RSC Advances

PAPER

View Article Online
View Journal | View Issue

Cite this: *RSC Adv.*, 2025, **15**, 6803

On the impact of aromatic core fluorination in hydrogen-bonded liquid crystals†

Ahmed F. Darweesh, *[a] Christian Anders,[b] B. S. Ranjitha,[c] G. Shanker[c] and Mohamed Alaasar *[ab]

Herein we report the impact of fluorine substitution on the liquid crystalline (LC) self-assembly of supramolecular hydrogen-bonded rod-like architectures. This was systematically investigated by introducing fluorine atom at different positions or with different numbers on the investigated supramolecules. Therefore, eight different groups of hydrogen-bonded LCs (HBLCs) were designed and synthesized in which four 4-hexyloxybenzoic acid derivatives without or with fluorine substitution were used as proton donors. The proton acceptors are fluorinated or nonfluorinated alkyloxyazopyridine derivatives. The hydrogen bond formation between the complementary components was proved using FTIR and ^{1}H NMR spectroscopy. All HBLCs were investigated for their mesomorphic behaviour using various tools such as differential scanning calorimetry (DSC), polarized optical microscopy (POM) and X-ray diffraction (XRD). Depending on the position and number of fluorine atoms different LC phases were observed including nematic, orthogonal non-tilted smectic A (SmA) or tilted smectic C (SmC) phases in addition to an unknown X phase. Depending on the position of the fluorine substitution, it was proved from the XRD investigations that different types of cybotactic nematic phases (N_{Cyb}) are exhibited by the reported HBLCs. Because of *cis–trans* photoisomerization under light irradiation of the reported HBLCs, their photo responsivity was investigated in solutions as well as between the different LC phases. This report provides key insights into the structure–property relationships of HBLCs, which might be of interest for optical storage device applications.

Received 28th January 2025
Accepted 24th February 2025

DOI: 10.1039/d5ra00670h

rsc.li/rsc-advances

1. Introduction

Non-covalent interactions are distinct from covalent ones and ensure functionality of biological systems such as proteins or DNA.[1] Among them, vital hydrogen bonding plays a crucial role in numerous instances in nature and biological systems,[2–5] driving the field of supramolecular chemistry and gives inspiration for material scientists to design interesting functional materials such as liquid crystals (LCs).[6]

Decisively, shape anisotropy, molecular interaction direction, and its strength support the achievement of LC phases and mesophase formation.[7,8] The advantage of using non-covalent interactions between two mesogenic or non-mesogenic components to produce LC materials is to avoid the many steps required for organic synthesis, thus reducing the total cost and environmental pollution.[9] The field of hydrogen-bonded liquid crystals (HBLCs) was initiated by Kato's group,[10] when first examples of HBLCs were reported between the 4-alkoxybenzoic acids as the proton donors and pyridine derivatives as the proton acceptors. Later various classes of HBLCs have been designed and prepared. These encompass low and high molecular weight calamitics,[11,12] bent-core molecules,[13–15] LC polymers,[16] and polycatenars,[17–19] with a broad application potential in technological fields.

Fluorine substitution in organic compounds exhibits captivating and unusual properties due to a combination of polar and steric effects, in addition to the strong covalent bond between fluorine and carbon, which imparts greater stability to the compounds.[20] The introduction of fluorine into distinct classes of LCs, including calamitics,[21,22] discotics,[23,24] bent-core,[25–27] LC polymers,[28,29] and other non-conventional LCs,[30] does not compromise the material's liquid crystal nature. As a result of its larger size compared to hydrogen, fluorine provides more steric hindrance and greater polarity, which affects the melting point, mesophase characteristics, and phase transition temperatures. To modify the liquid crystalline behaviour, fluorine could be added at various positions in the molecular structure of a given mesogen. Therefore, fluorine was used in perfluorinated terminal chains,[31–33] in the aromatic backbone as an ending group[34,35] or as a lateral group at

[a]*Department of Chemistry, Faculty of Science, Cairo University, 12613 Giza, Egypt. E-mail: darweesh@sci.cu.edu.eg*

[b]*Institute of Chemistry, Martin Luther University Halle-Wittenberg, 06120 Halle, Germany. E-mail: mohamed.alaasar@chemie.uni-halle.de*

[c]*Department of Chemistry, Bangalore University, Jnana Bharathi Campus, Bengaluru, 560056, India*

† Electronic supplementary information (ESI) available. See DOI: https://doi.org/10.1039/d5ra00670h

different positions.[22,36–38] These distinct forms of molecular tailoring play a crucial role in unravelling fundamental structure–property relationships and developing materials tailored for various applications. Recently, fluorinated rod-like molecules were found to exhibit the ferroelectric nematic phase in addition to other polar LC phases.[39–41]

Most of the HBLCs incorporate azopyridine derivatives as proton acceptors.[42–47] Azopyridines demonstrate appealing characteristics, including their ability to act as promesogenic material and undergoing *trans–cis* photoisomerization upon light irradiation. These traits render them extremely valuable in the domain of photonics applications.[48–52]

Previously, we have reported the effect of mono aromatic core fluorination in the azopyridine derivatives used as hydrogen-bond acceptor on the LC behaviour of rod-like molecules.[53] However, fluorination of the proton donor *i.e.* the benzoic acid derivatives with different degrees is not investigated yet. Therefore, herein we investigate systematically the impact of aromatic core fluorination with different number and positions on the liquid crystalline behaviour of HBLCs. For this purpose, two different types of azopyridine derivatives (**AH*n*** and **AF*n***, Fig. 1) were used as the proton acceptors, while the proton donors are 4-hexyloxybenzoic acid (**B6H**) and its fluorinated derivatives (**B6F$_2$**, **B6F$_3$** and **B6F$_{23}$** Fig. 1).

Therefore, eight different combinations between these components were achieved resulting in total of 32 HBLCs (**HHH*n*–FFF*n***, Scheme 1). The effect of varying the terminal chain length attached to the proton acceptor (**AH*n*** or **AF*n***) on the LC behaviour was also investigated (n = 8, 10, 12, 14). Moreover, the *trans–cis* photoisomerization of the reported materials were studied in solution as well as between different LC phases. This wide variety of molecular building blocks allows a systematic study of structure–property relationships and provide photo-switchable functional materials which could be of interest for applications in thermo-responsive optical filters and sensors.[54]

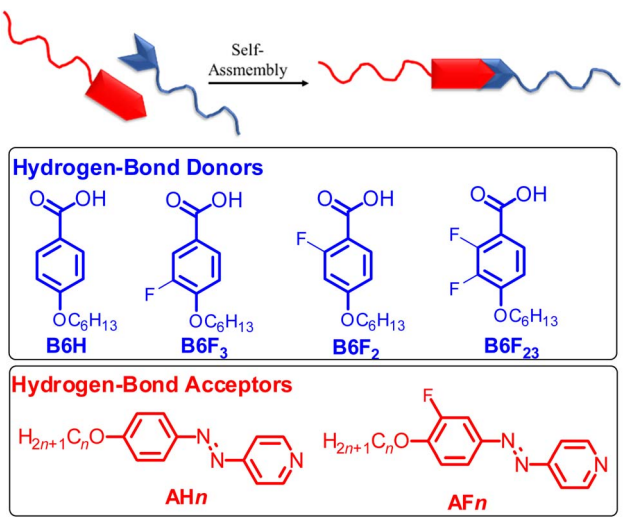

Fig. 1 Model of HBLCs and the chemical structures of hydrogen-bond donors and hydrogen-bond acceptors under discussion.

2. Synthesis

The synthesis of the target materials was performed as illustrated in Scheme 1. The proton acceptors *i.e.* the azopyridine derivatives with or without fluorine substitution (**AH*n*** and **AF*n***) were synthesized using previously reported protocols.[19,43,55] The proton donors with different degree of fluorination were synthesized starting from different key intermediates using standard reported procedures,[56,57] while the non-fluorinated 4-hexyloxybenzoic acid **B6H** was commercially available. The general synthetic procedures and analytical data for the synthesized intermediates and target molecules are provided in ESI.†

3. Results and discussion

3.1. Analysis of the hydrogen-bond formation

To identify the hydrogen bond formation between the complementary components – the benzoic acid derivatives and the azopyridines – we conducted both FTIR measurements using the conventional KBr method and NMR analysis for some selected examples. As a representative example the FTIR spectra of the supramolecule **HHH12** (green curve) and its components **B6H** (blue curve) and **AH12** (red curve) are presented in Fig. 2a and b (for the complete spectra refer to Fig. S12a†).

As is evident from Fig. 2a, the FTIR bands of the supramolecule **HHH12** differ significantly from those of the pure components. The broad band observed in the range of 2500–3300 cm^{-1} for **B6H**, due to the formation of carboxylic dimer, is diminished in **HHH12**. Instead, two new broadened bands centred at approximately 2445 and 1929 cm^{-1} appear in **HHH12**, which is ascribed to Fermi resonance overtone.[53] Additionally, the band at 1686 cm^{-1} corresponding to $\nu_{C=O}$ stretching vibration of the pure acid (**BH6**), broadens, decreases in intensity, and shifts to a higher wavenumber (~1696 cm^{-1}) upon complexation with the azopyridine **AH12** (Fig. 2b).

These observations align with previously reported hydrogen-bonded systems involving pyridine derivatives and benzoic acids,[53,58,59] confirming the successful hydrogen-bond formation between the azopyridine derivative **AH12** and the acid **BH6**.

Next, the FTIR spectra for **HHH12** and its related analogues with varying numbers and positions of fluorine substitutions were also recorded, and the results are given in Fig. S13–S18.† This investigation aimed to study how the strength of the hydrogen bond could be influenced by the position and degree of core fluorination. Regardless of the number or position of the fluorine atoms, the formation of H-bonds between each azopyridine derivative and the benzoic acids was successfully confirmed. In all cases, the two bands resulting from the Fermi resonance overtone were observed, along with changes in the intensity and wavenumber of the carbonyl band ($\nu_{C=O}$) of the pure acids compared to their complexed form (Fig. S13–S18†).

Table 1 summarizes the wavenumber shifts ($\Delta\nu_{C=O}$) calculated between the $\nu_{C=O}$ band for the pure acids and their corresponding supramolecules. As shown in Table 1, the lowest $\Delta\nu_{C=O}$ value is calculated for the nonfluorinated supramolecule **HHH12**. Introducing one fluorine atom at the *ortho* position

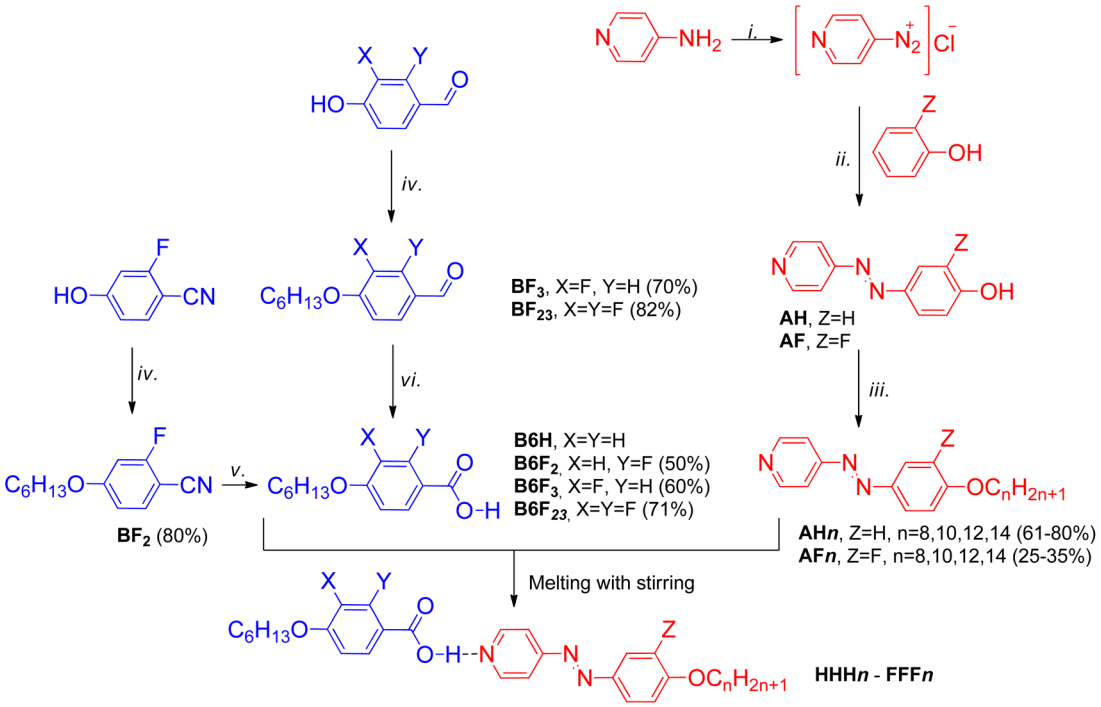

Scheme 1 Synthesis of the new HBLCs **HHH*n*–FFF*n***. Reagents and conditions: (i) $NaNO_2$/HCl/H_2O, 0 °C, 5 h; (ii) NaOH, $NaHCO_3$; (iii) BrC_nH_{2n+1}, K_2CO_3, DMF, 80 °C, 18 h; (iv) BrC_6H_{13}, K_2CO_3, *n*-Bu_4NI, butanone, reflux, 5 h; (v) KOH, ethanol, reflux, HCl; (vi) resorcinol, *t*-butanol, $NaOCl_2$, $NaH_2PO_4 \cdot 2H_2O$, stirring, r.t., HCl.

with respect to the alkoxy chain in the azopyridine derivative **AH12** in case of **HHF12** results in no change in $\Delta\nu_{C=O}$ compared to **HHH12** (Fig. S13†). This is because the fluorine atom is positioned far from the interacting carboxylic group, thus having almost no effect on the strength of the formed hydrogen bond.

On the other hand, shifting the F atom from the azopyridine derivative to the benzoic acid derivative, while maintaining its *ortho* position relative to the terminal alkoxy chain in case of **FHH12**, resulted in a more pronounced effect (Fig. S14†). The $\Delta\nu_{C=O}$ value for **FHH12** is ~24 and 22, indicating that the formed H-bond in this case is stronger compared to those in **HHH12** or **HHF12**. This can be attributed to the electron-withdrawing effect of the fluorine atom, which increases the acidic character of the proton donor (**B6F$_3$**). Similar $\Delta\nu_{C=O}$ values were also recorded for **FHF12**, further confirming that the fluorine atom on the azopyridine derivative has no significant effect on the strength of hydrogen bond.

Finally, introducing a fluorine atom adjacent to the carboxylic group (**HFH12** or **HFF12**) or using two F atoms (**FFH12**) resulted in similar $\Delta\nu_{C=O}$ values in all cases ~17. This suggests that for all fluorinated supramolecules constructed using any of the fluorinated benzoic acid derivatives (**B6F$_3$**, **B6F$_2$** or **B6F$_{23}$**) higher $\Delta\nu_{C=O}$ values could be calculated compared to the supramolecules derived from the nonfluorinated acid **BH6** or the fluorinated azopyridine derivative **AF12**. This indicates that fluorine substitution on the benzoic acid side results in a more stabilized hydrogen bond formation.

To confirm the formation of the hydrogen bond in solution, we have also investigated some selected supramolecules using ^{1}H NMR spectroscopy. Fig. 3 represents the ^{1}H NMR of **HHH12** (black) without fluorine substitution, alongside the spectra of its precursor acid **B6H** (blue) and the azopyridine derivative **AH12** (red) in the aromatic region. The results reveal distinct signal differences between the pure components and their mixed state. In the supramolecule **HHH12**, the ^{1}H NMR spectrum shows an increase of the chemical shift of the pyridine ring protons of **AH12**, as well as the signals of the two protons next to the azo group in the benzene ring. Additionally, a slight shift in the chemical shift values for **B6H** protons upon complexation with **AH12** could be observed. These spectral changes confirm the successful formation of hydrogen bond between the complementary components in chloroform.

To further investigate the influence of fluorine on the strength of the hydrogen bond, we examined **FFH12**, which features double fluorine substitution on the benzoic acid derivative (Fig. 4), and **FHH12**, which has single fluorine atom instead of two (Fig. S21† in the ESI). As can be seen from Fig. 4, the increase of the chemical shift values of all **AH12** protons after hydrogen formation (**FFH12**, black spectrum) is more pronounced compared to that observed in the nonfluorinated supramolecule (**HHH12**, Fig. 3). This is due to the stronger interaction between the double fluorinated acid **B6F$_{23}$** and **AH12**. Additionally, the change in the shape of the signals for the two protons of the **B6F$_{23}$** after complexation further supports this conclusion.

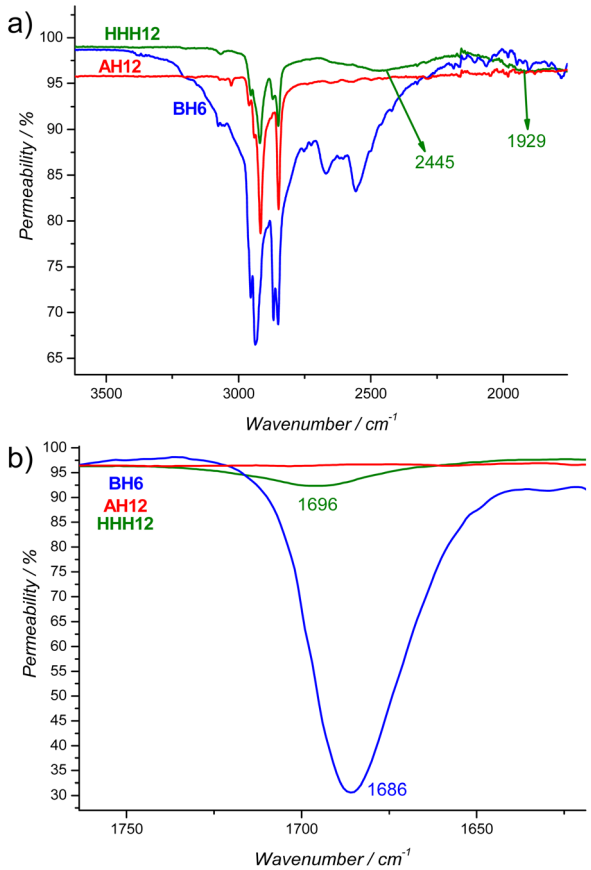

Fig. 2 FTIR spectra of the supramolecule **HHH12** (green) and its complementary components **B6H** (blue), **AH12** (red) in the crystalline state at room temperature enlarged area (a) between 1750 cm^{-1} and 3600 cm^{-1} and (b) between 1620 cm^{-1} and 1760 cm^{-1}.

Table 1 FTIR carbonyl bands at room temperature for selected supramolecules and its corresponding pure acid components[a]

Pure acid	$\nu_{C=O}$ cm^{-1}	Supramolecule	$\nu_{C=O}$ cm^{-1}	$\Delta\nu_{C=O}$
B6H	1686	**HHH12**	1696	10
B6H	1686	**HHF12**	1696	10
B6F$_3$	1667, 1681	**FHH12**	1691, 1703	24, 22
B6F$_3$	1667, 1681	**FHF12**	1691, 1703	24, 22
B6F$_2$	1676	**HFH12**	1693	17
B6F$_{23}$	1681	**FFH12**	1698	17
B6F$_2$	1676	**HFF12**	1693	17

[a] $\Delta\nu_{C=O}$ represents the change in the carbonyl band of the pure acid component upon complexation with the azopyridine derivative.

Similar trends were also observed in the ^{1}H NMR spectra of **FHH12** when compared to its pure components, **B6F$_3$** and **AH12** (Fig. S21† in the ESI). These findings lead to the conclusion that fluorination of the proton donor *i.e.* the benzoic acid derivative enhances the interaction between the two components, resulting in stronger hydrogen bond formation. Moreover, it confirms the stability of the hydrogen bond formation in solution.

3.2. Mesomorphic behaviour of synthesized HBLCs

Before discussing the LC behaviour of the target HBLCs we should refer to the fact that all azopyridine derivatives used in this work with or without fluorine are nonmesomorphic materials and melts directly to the isotropic liquid state.[19,53] On the other hand, the benzoic acid derivatives are either nematogenic or crystalline materials as indicated by POM investigations. The transition temperatures of the proton donors as well as for the proton acceptors are summarized in Tables S1 and S2,† respectively. Therefore, the observation of different mesophases in the HBLCs under POM could be considered as a further indication of the formation of the hydrogen-bonded supramolecular complexes.

The synthesized complementary components *i.e.* the benzoic acid derivatives and the azopyridine derivatives were used to prepare eight different groups of supramolecular HBLC complexes, which differ from each other's in the degree and position of fluorine substitution (Scheme 1). The formation of the hydrogen-bonded supramolecular complex between the complementary components was further confirmed by DSC investigations. For example, Fig. 5 shows the DSC heating and cooling cycles for the supramolecular complex **FHH8** and its complementary components the 3-fluoro-4-*n*-hexyloxybenzoic acid (**B6F$_3$**) and the 4-(4-octyloxyphenylazo)pyridine (**AH8**). Upon mixing the two components the individual transition temperatures recoded for each of them before mixing totally disappeared (red and blue curves in Fig. 2) and new transition temperatures are exhibited by the formed HBLC (green curves in Fig. 2). This clearly indicates the formation of the hydrogen bond between **AH8** and **B6F$_3$** yielding the desired HBLC **FHH8**. Similar investigations were performed for all synthesized HBLCs (Tables S3–S10 and Fig. S22–S29† in ESI for additional DSC traces) and the results confirm the successful formation of the supramolecular complexes in all cases.

The phase behaviour of all prepared supramolecules is represented graphically in Fig. 6 and the numerical data for transition temperatures and the corresponding enthalpy values are given in Table S3–S10† in the ESI.

Non-fluorinated HBLCs. To investigate the dependence of the LC behaviour of the reported HBLCs on the degree of core fluorination and its position, it was necessary to start first with the nonfluorinated HBLCs (**HHH*n***) constructed between the non-substituted benzoic acid (**B6H**) and the azopyridines (**AH*n***). This series is considered as a reference for comparison with remaining synthesized HBLCs. As can be seen from Fig. 6a, **HHH*n*** series displays three different types of LC phases, which are enantiotropic ones in all cases (Table S3†). On cooling the shortest member **HHH8** from the isotropic state a transition to a Schlieren textures is observed (Fig. 7a), which flashes under shearing. This is typically observed for nematic (N) phase and therefore this phase is assigned as N one. The N phase was exhibited by the proton donor *i.e.* **B6H** over relatively wide range ~30 K. Upon formation of supramolecule **HHH8** by mixing **B6H** with **AH8** the N phase is retained for shorter range ~10 K and additional phase is induced with wide range of ~18 K on heating and ~24 K on cooling (Table S3†). This lower

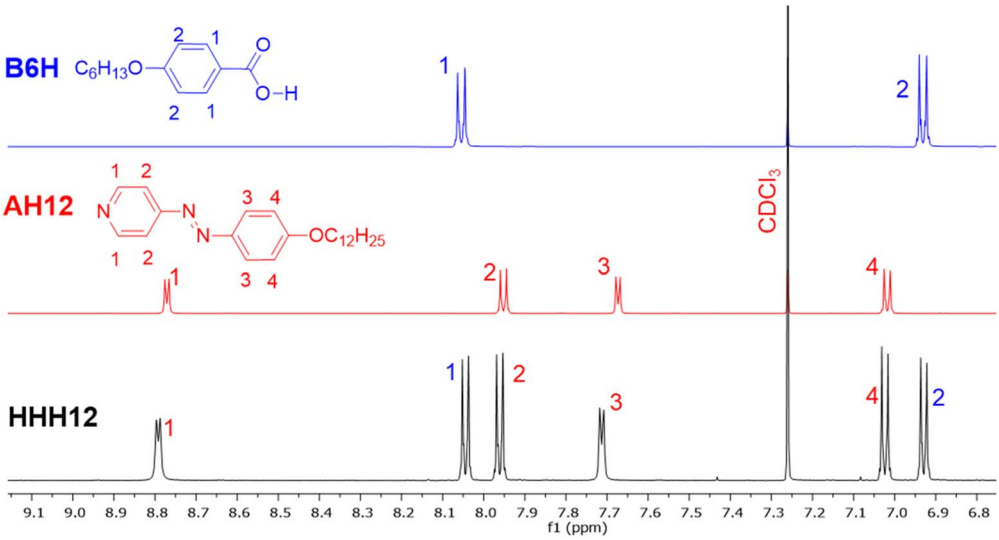

Fig. 3 ^{1}H NMR spectra (500 MHz, $CDCl_3$) of the supramolecule **HHH12** (black) and its complementary components the azopyridine derivative **AH12** (red) and the benzoic acid derivative **B6H** (blue) in the aromatic region (for the whole range see Fig. S19† in the ESI).

temperature LC phase is characterized by the appearance of homeotropic areas and broken fan shaped textures (Fig. 7b), which are known for the uniaxial non-tilted smectic A (SmA) phase and therefore this phase is designated as SmA phase. The transition between N and SmA phases could be also detected by DSC investigations (Table S3 and Fig. S22†).

The N phase is retained for the next homologue **HHH10** but with shorter range followed by wide range of SmA phase. Notably, for all members with $n \geq 10$–14 both melting and crystallization temperatures are lowered compared to **HHH8** resulting in wider LC range. For the supramolecules with $n = 12$ and 14 the N phase totally disappeared and the SmA phase is retained. Interestingly, an additional LC phase is observed below the SmA for **HHH12** and **HHH14**, which cannot be detected by DSC investigations (Table S3†) indicating a second order phase transition. This phase is characterized by its high birefringence in all areas and the appearance of Schlieren texture with four-brush disclinations (indicated by white circle in Fig. 7c). These observations are characteristic for the synclinic tilted smectic C phase.

Mono fluorinated HBLCs. Introducing one fluorine atom in the aromatic core leads to formation of the supramolecules **HHF*n***, **FHH*n*** and **HFH*n***. It is interesting that the position of F atom in such HBLCs plays an important role in the displayed LC phases in each case. For the first series **HHF*n*** having the F atom at *ortho* position with respect to the terminal alkoxy chain in the azopyridine derivatives (**AF*n***), the melting temperatures are slightly affected compared to those of **HHH*n*** supramolecules

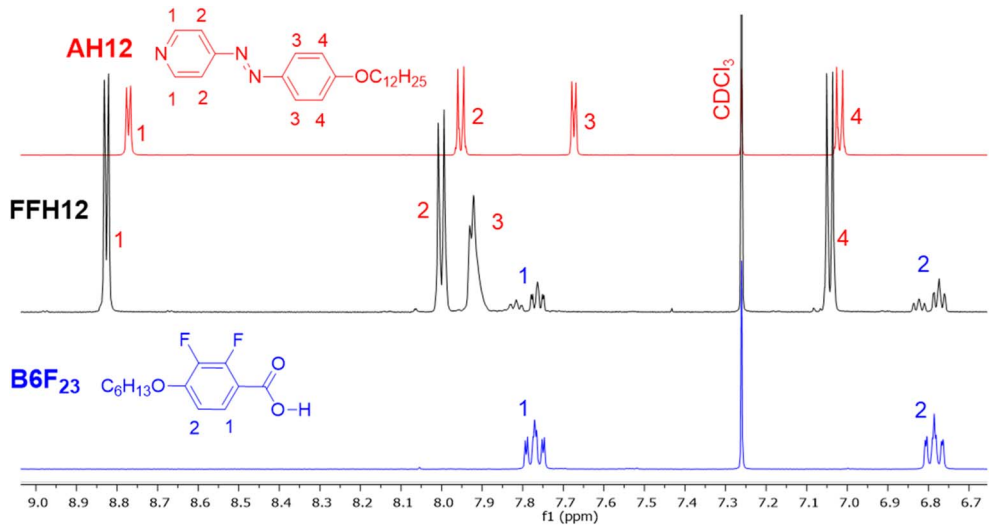

Fig. 4 ^{1}H NMR spectra (500 MHz, $CDCl_3$) of the supramolecule **FFH12** (black) and its complementary components the azopyridine derivative **AH12** (red) and the benzoic acid derivative **B6F$_{23}$** (blue) in the aromatic region (for the whole range see Fig. S20† in the ESI).

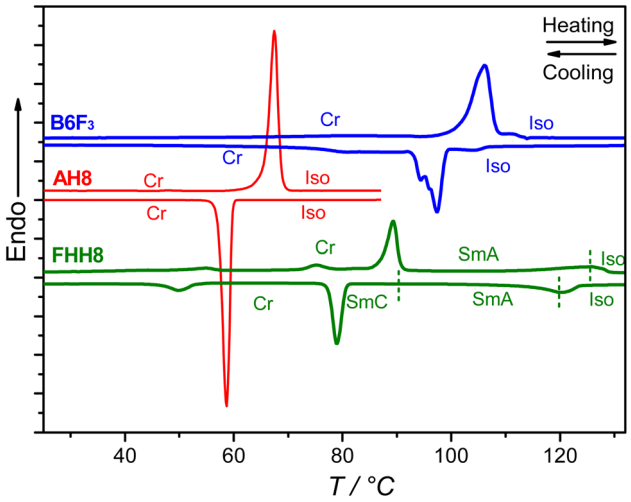

Fig. 5 DSC Heating and cooling cycles of the HBLC **FHH8** (green curves) and its individual components, the proton donor **B6F$_3$** (blue curves) and the proton acceptor **AH8** (red curves) at a scanning rate of 10 K min^{-1}.

(see Tables S3 and S4†). On the other hand, the clearing temperatures are reduced because of the steric effect of the F atom (Fig. 6b and Table S4†). Moreover, the nematic phase is the only observed LC phase for the shortest homologue. The range of this N phase is decreasing with increasing n accompanied by the appearance of SmC with chain elongation. For the longest homologue **HHF14** the N phase is totally removed and the SmC phase is the only observed mesophase (Fig. 6b).

Changing the F position from the azopyridine derivative side to be on the other terminal of the supramolecule *i.e.* at *ortho* position in the benzoic acid derivative (**B6F$_3$**) leads to the HBLCs **FHH*n*** (Fig. 6c and Table S5†). Interestingly, this modification results in different phase sequences compared to their related HBLCs **HHF*n***, where the N phase is totally removed and instead a SmA phase is observed for all members of **FHH*n*** (compare Fig. 6b and c). On the other hand, the SmC is observed for a small range in case of **FHH8** and its range is increasing upon chain elongation. The loss of N phase and appearance of smectic phases in **HHF*n*** is an indication for favouring layer structure in such HBLCs, which is a result of increasing core–core interaction. This indicates that the strength of the hydrogen bond between the complementary components in these HBLCs plays an important role in determining the type of LC phases. Introducing F in the benzoic acid derivative increases its character as proton donor, meaning stronger H-bonding interaction and more core–core interaction leading to the observed lamellar phases (SmA and SmC phases). In contrast, introducing the F at the azopyridine derivative (**HHF*n***) does not affect the H-bonding strength to the same extent compared to that in case of **FHH*n*** because it is far from the two interacting positions. Instead, because of its steric effect the lamellar structure is only favoured with chain elongation and the nematic phase is retained for homologues with $n \leq 12$ (Fig. 6b). This hypothesis is supported by the observed phase sequences in case of the next mono fluorinated HBLCs *i.e.* **HFH*n***. The later have the F atom in inner position instead of outer one in case of **FHH*n***, which results in more steric interaction leading to the formation of N phases in all **HFH*n*** homologues (Fig. 6e and 8). The N phase is the only observed mesophase for the shortest homologue and on chain elongation its range is decreasing and become very short for the longest chain homologue (**HFH14**). More interesting for all **HFHn** with $n \geq 10$ a different LC phase characterized by its homeotropic texture with bright lines (Fig. 8c) is observed below the N phase. The range of this phase is increasing with chain elongation (Table S7†). Based on XRD results (Section 3.3), the exact type of this LC phase cannot be solved and therefore it is assigned as X phase. From these observations, it could be concluded that changing the position of the F atom not only alters the LC range or sequence but also changes the type of LC phases.

Double fluorinated HBLCs. Aiming to investigate the effect of double core fluorination on the phase behaviour of the neat supramolecules **HHH*n***, we synthesized additional three groups having two fluorine atoms at different positions (**FHF*n***, **FFH*n*** and **HFF*n***). Combining the two individual components having the F atom at *ortho* positions with respect to the terminal chains results in **FHF*n*** series (Fig. 6d). This group of HBLCs have lower clearing temperatures compared to the mono fluorinated HBLCs (**HHF*n*** and **FHH*n***), because of increased steric effect caused by introducing two F atoms instead of one. However, all members of **FHF*n*** are liquid crystalline materials displaying three enantiotropic LC phases. The shortest homologue **FHF8** exhibits the phase sequence of SmC–SmA–N (Fig. 6d), meaning that using two F atoms in these HBLCs could lead to polymesomorphism as compared to the related analogues **HHF8** and **FHH8** (Fig. 6b and c). On chain elongation the N phase is completely removed and both SmA and SmC phases are retained till $n = 14$. The same trend was observed by changing the F from the azopyridine side to be in the *meta* position of the benzoic acid derivative *i.e.* by using the double fluorinated benzoic acid derivative **B6F$_{23}$** as the proton donor and **AH*n*** as proton acceptors. This results in the **FFH*n*** series having also SmC–SmA–N phase sequence for the shortest member **FFH8** and SmC–SmA sequence for the next homologue (**FFH10**). For the next two homologues the SmC phase is the only observed mesophase in relatively wide temperature range. Interestingly, the clearing temperatures of **FFH*n*** series are comparable to those of the non-fluorinated HBLCs (**HHH*n***) which is not a common feature of lateral fluorine substitution in rod-like LCs. This result in wider LC phase ranges for **FFH*n*** members compared to **FHF*n***.

Changing the position of the F atom in **FHF*n*** from the *ortho* position in the benzoic acid derivative to be in a *meta* position *i.e.* using **B6F$_2$** as the proton donor leads to the **HFF*n*** series (Fig. 6f). This results in more steric interactions, leading to disfavouring of layer structures. Therefore, the N phase is observed for all members with $n \geq 8$–12 and for the longest homologue the N phase is totally removed and SmC–SmA phase sequence appeared. More interesting, for **HFF12** two different types of N phases are observed as indicated from the POM investigations (Fig. 9). Both N phases exhibit Schlieren textures, which flashes on applying shearing stress confirming the

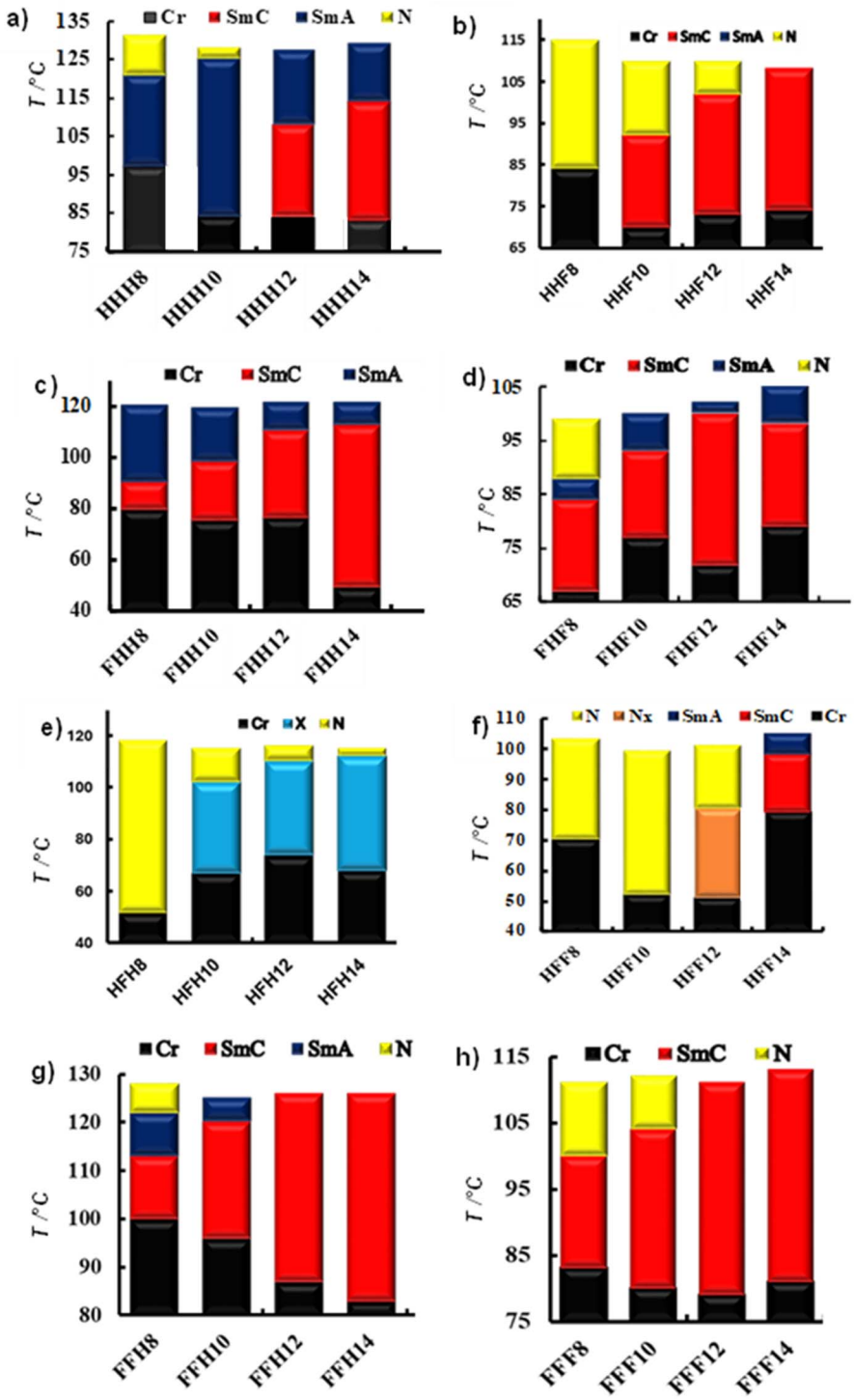

Fig. 6 Schematic illustration of combined DSC and POM data on cooling at a rate of 10 K min^{-1} for the synthesized HBLCs. N = nematic phase, SmA = smectic A, SmC = smectic C, X = unknown LC phase; Nx = nematic x phase.

nematic nature. Unfortunately, it was not possible to further investigate the lower temperature N phase with XRD due its monotropic nature and therefore it is assigned as Nx phase.

Triple fluorinated HBLCs. The last group of synthesized HBLCs was **FFF*n*** series having three F atoms (Fig. 6h). This series was constructed using the double fluorinated benzoic acid derivative **B6F$_{23}$** and the fluorinated azopyridines **AF*n***. As can be seen from Fig. 6h all members of this series are LC materials with the phase sequence of SmC–N for $n = 8$ and 10 and only SmC phase for $n = 12$ and 14 (Fig. 9c and Table S10†). Therefore, using three F atoms does not suppress the LC formation but instead modifies the LC phase types and results

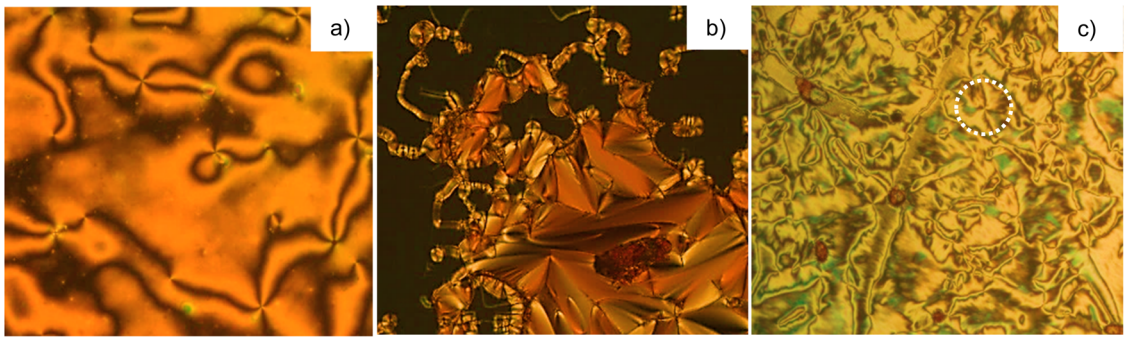

Fig. 7 POM textures observed for: (a) **HHH8** in the nematic phase at 128 °C, (b) **HHH14** in the SmA phase at 120 °C and (c) **HHH12** in the synclinic SmC phase at 105 °C.

mainly in tilted layer structures (SmC phase) with relatively wide ranges.

These results give insights about the structure–property relationship in these HBCLs and emphasizes the role of aromatic core fluorination, its degree and position as key factors in determining and controlling the LC phase types and ranges. This strategy could be used as a successful tool for advancing new materials for certain type of applications.

3.3. X-ray diffraction (XRD) investigations

To prove the different types of LC phases observed for the synthesized HBLCs we have performed XRD investigations for some selected examples. All experiments were performed using a surface-aligned sample, prepared by slow cooling of a small drop of the sample on a glass substrate from the isotropic liquid state.

The first example is the nonfluorinated supramolecule **HHH14**, which display two LC phases as confirmed from POM investigations. In the wide-angle region (WAXS) a broad diffuse scattering in temperature range of the lower temperature LC phase with d value $\sim$ 0.44 nm is observed at $T \sim 100$ °C (see the inset in Fig. 10a). This indicates a liquid crystalline phase with no fixed positions of the supramolecules. In the small-angle region (SAXS) at the same temperature a sharp peak is observed at $2\theta \sim 2.19°$ indicating a layer structure with a second order peak at $2\theta \sim 4.34°$ (Fig. 10a). The calculated d value is $\sim$4.04 nm which is smaller than the molecular length of **HHH14** calculated with Materials Studio for all-*trans* conformation of the alkyl chains ($L_{mol} = 4.44$ nm). This indicates the presence of a tilted SmC phase with a tilt angle β of $\sim$24.5° calculated according to $\cos\beta = d/L_{mol}$. In the higher temperature LC phase (Fig. 10b), the WAXS region still shows a wide diffuse scattering confirming the transition from the SmC phase to another LC phase. In the SAXS region the first and second order reflections could be also seen proving the presence of another lamellar LC phase with a d value $\sim$ 4.13 nm, which is larger than that calculated for the SmC phase. These results confirm the presence of SmA phase with partial intercalation of the aromatic cores at higher temperature for **HHH14**, which agrees with the homeotropic, and fan-shaped textures observed under POM (Fig. 7b).

The next example is the monofluorinated **HFH10** supramolecule. On cooling **HFH10** from the isotropic liquid and at $T \sim 110$ °C a diffuse wide-angle scattering (WAXS) reflex at $d =$ 0.44 nm is observed confirming its LC nature (Fig. 11a). The SAXS pattern recorded at the same temperature shows one scattering peak at $2\theta \sim 2.36°$. The peak is relatively sharp, and its intensity increased with decreasing temperature in the N phase. The appearance of such sharp peak in the N phase is not common for rod-like molecules, which usually display a broad halo scattering.[60] This peak corresponds to d value of $\sim$3.74 nm, which is lower the molecular length of the compound calculated with Materials Studio for all-*trans* conformation of the alkyl

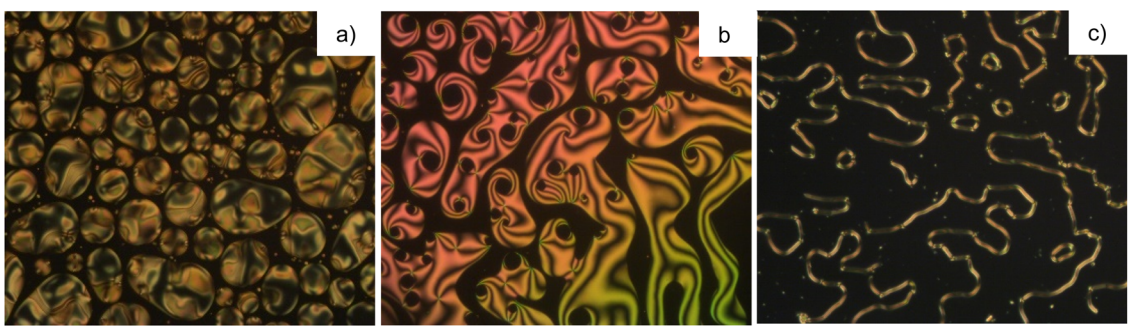

Fig. 8 POM textures observed for: (a) nematic droplets of **HHF10** at the transition from the isotropic liquid phase at 115 °C; (b) nematic phase of **HHF12** at 116 °C; (c) unknown phase of **HFH10** at 90 °C.

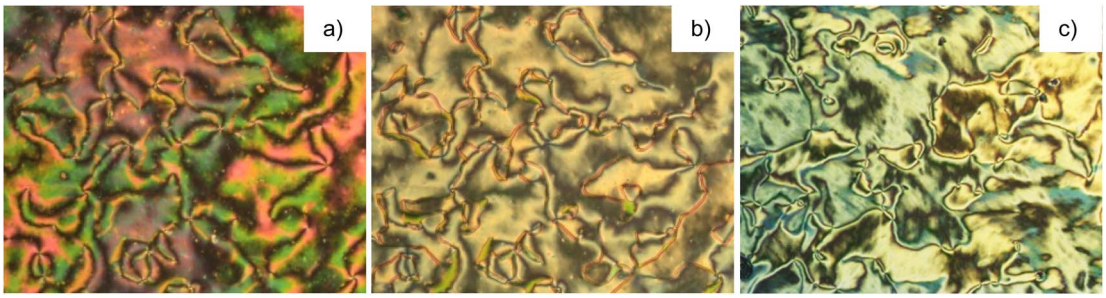

Fig. 9 POM textures observed on cooling for: (a) N phase of **HFF12** at 95 °C, (b) Nx phase of **HFF12** at 70 °C and (c) the SmC phase of **HFF14** at 96 °C.

chains $L_{mol} = 4.09$ nm. The presence of this peak and the *d*-value suggest the presence of cybotactic clusters of Sm-like structure (Cyb) in the nematic phase of **HFH10** and therefore the nematic phase could be assigned as N_{Cyb} one. Such N_{Cyb} phase was reported recently for few examples of rod-like LC phases.[33,61–65] The N_{Cyb} phase was also proved for the supramolecule **HFF8** from XRD investigations (see Section 2 in the ESI†).

At the transition to the next LC phase on further cooling of **HFH10** the single peak recorded in SAXS at $T \sim 98$ °C become sharper with $d \sim 3.88$ nm and a second reflex at $2\theta \sim 2.67°$ (Fig. 10b). The calculated *d*-value is larger than that observed in the N_{Cyb} phase and less than the molecular length ($L_{mol} = 4.04$ nm). This inline was the presence of titled lamellar phase. However, based on the observed texture under POM given in Fig. 8c and the second small reflection at $2\theta \sim 2.67°$, which are not typical for known SmC phases, the exact structure of this lower temperature LC phase cannot be solved at the current stage and therefore it is assigned as X phase.

It should be noted that the observation of N_{Cyb} phase in the investigated supramolecules as confirmed from XRD investigations, indicates that different types of nematic phases are exhibited by the reported supramolecules. Therefore, depending on the adjacent LC phase the nematic phase of series **HHH*n*** could be assigned as N_{CybA} phase formed by cybotactic clusters of the SmA type, while that of **HHF*n*** series is N_{CybC} formed by SmC clusters. The third type is the N_{CybX} phase adjacent to the unknown X phase in **HFH*n*** supramolecules. This proves that the position of the fluorine substitution plays a very important role in determining the type of the cybotactic clusters present in such nematic phases.

3.4. Photo-responsive behaviour

The focus of the current work was not only on the structure–property relationships of HBLCs by correlating the results discussed in the previous sections from DSC, POM, FTIR, ^{1}H NMR and XRD but also to investigate the photo-responsive behaviour of the reported HBLCs. We designed the HBLCs to be photo-responsive because of the *trans–cis* photoisomerization of the azopyridine unit upon light irradiation. Therefore, to investigate the effect of fluorine substitution on the photo-isomerization in solution we have selected the HBLCs with $n = 8$ from all series for such study (Fig. 12a–h).

All selected HBLCs were dissolved in chloroform ~2 mg/10 mL and measured with UV-vis spectrometry before and after UV illumination with time intervals of 5 seconds. Before UV irradiation all materials exhibit a strong absorption band

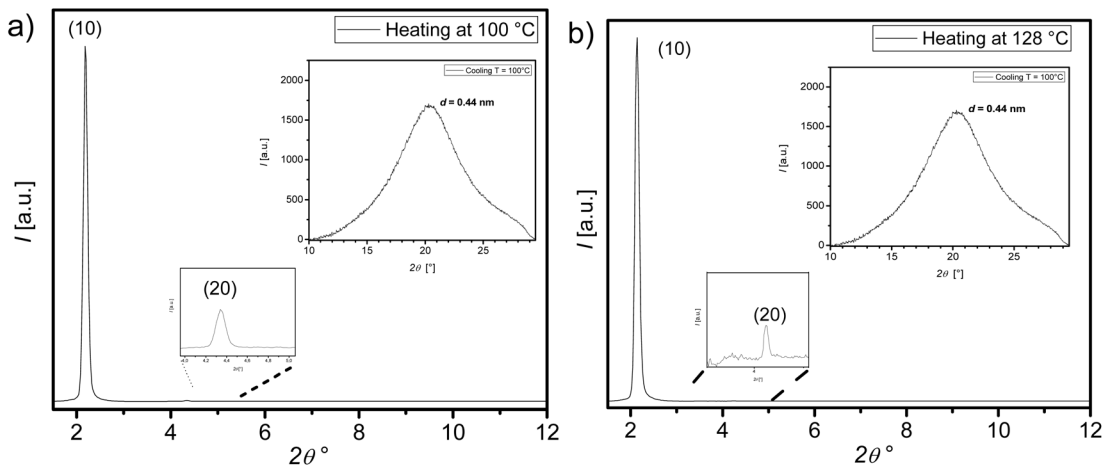

Fig. 10 Plot of the integrated scattered intensity as a function of 2θ in the small-angle region (SAXS) for **HHH14**: (a) the SmC phase at $T = 100$ °C and (b) the SmA phase at $T = 128$ °C. The insets in (a) and (b) show the WAXS region in both phases.

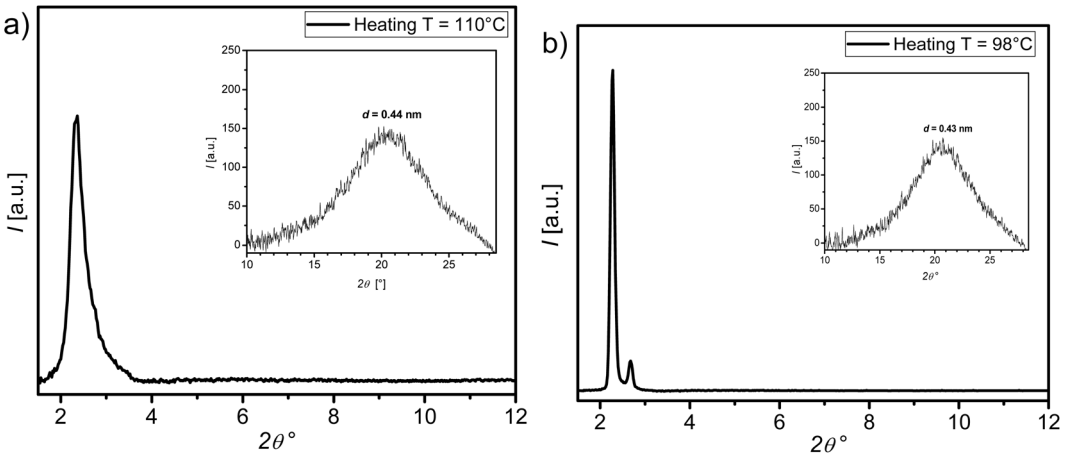

Fig. 11 Plot of the integrated scattered intensity as a function of 2θ in the small-angle region (SAXS) for **HFH10** on cooling: (a) the N phase at $T =$ 110 °C, (b) the X phase at $T = 98$ °C. The insets in (a) and (b) show the WAXS region in both phases.

between 355–358 nm, resulting from the π–π* transition. This indicates the presence of the stable *trans* isomer. After irradiation with UV light different behaviour is observed for the HBLCs, which depends strongly on the degree and position of fluorine atoms. Therefore, for the nonfluorinated complex **HHH8** there is a slow transformation to the *cis* isomer with time, indicated by the decreasing of the initial absorption band at 355 nm and the appearance of another weak band around 448 nm. The latter is due to the n–π* transition, which corresponding to the *cis* isomer. These observations confirm the *trans–cis* photoisomerization of **HHH8** under UV irradiation. Introducing a fluorine atom at *ortho* position with respect to the terminal chain in the azopyridine derivative in case of **HHF8**, results in faster *trans–cis* photoisomerization as indicated by the less time required for reducing the band at 357 nm (Fig. 12b). Changing the F atom to the other end at the complex in case of **FHH8** suppress the photoisomerization completely as almost no change in the absorption band at 357 nm is observed. Using two F atoms at both terminals (X = Z = F, **FHF8**) results in a very similar behaviour to that of **HHF8**.

This process is more pronounced when the F atom is used next to the carboxylic group in the benzoic acid derivative (**HFH8**), which shows the fastest photoisomerization among all investigated HBLCs. For the remaining two complexes having two fluorines X, Y = F (**FFH8**) or three fluorines X, Y, Z = F (**FFF8**), no significant difference could be observed, where a slow photoisomerization process is observed in both cases. Therefore, from this investigation it could be concluded that compared to the nonfluorinated supramolecule (Fig. 12a) the *trans–cis* photoisomerization of mono fluorinated HBLCs strongly depend on the position of the F atom. Therefore, to reduce the *trans–cis* photoisomerization time the F atom should be introduced at outer position on the azopyridine side (Fig. 12b) or inner position on the benzoic acid side (Fig. 12e) instead of using it on outer position on the acid side (Fig. 12c). If the supramolecule contain two F atoms then at least one of them should be positioned at the azopyridine side (Fig. 12d and f) instead of having both of them at the acid side (Fig. 12g). In the latter case the *trans–cis* photoisomerization needs longer time, which is comparable to the triple fluorinated supramolecule (Fig. 12h). These different behaviours could be attributed to the steric effects resulting from using fluorine atoms at different positions. Keeping the measured solutions for all supramolecules in dark overnight and measuring them again results in almost identical spectra observed for the freshly prepared ones before light irradiation. This confirms that the *trans–cis* photoisomerization is completely a reversible process.

We have selected the supramolecules **HHH8** and **FFH8** as representative examples to investigate the photoisomerization between the different types of LC phases (Fig. 13). Isothermal UV light irradiation (365 nm) of the N phase of **HHH8** at $T =$ 125 °C results in a rapid transition to the isotropic liquid phase within three seconds (Fig. 13a and b). On removing the light source, the N phase texture is retained immediately, indicating a fast and reversible photo switching between N and isotropic liquid phase. This is a result of *trans–cis* photoisomerization, whereby the bent-shaped *cis*-isomer tends to destabilize the N phase, thus inducing a phase transition to the isotropic state. Similar observations were also observed between N and SmA (Fig. 13c and d) as well as between SmC and SmA (Fig. 13e, f) phases of **FFH8**. However, these transitions are slower (~7 seconds) compared to that between N and isotropic states in case of **HHH8**. This might be attributed to the higher order of the SmA and SmC phases, resulting in lower mobility of the mesogens in these LC phases compared to the less order found in the N phase. These observations could be of interest for applications such as optical information storage device applications and non-linear optics.[48,65]

4. Conclusion

This study provides a comprehensive exploration of the structure–property relationships in hydrogen-bonded liquid crystals (HBLCs), with a particular focus on the impact of aromatic core fluorination on their self-assembly and phase behaviour. By systematically varying the number and positions of fluorine

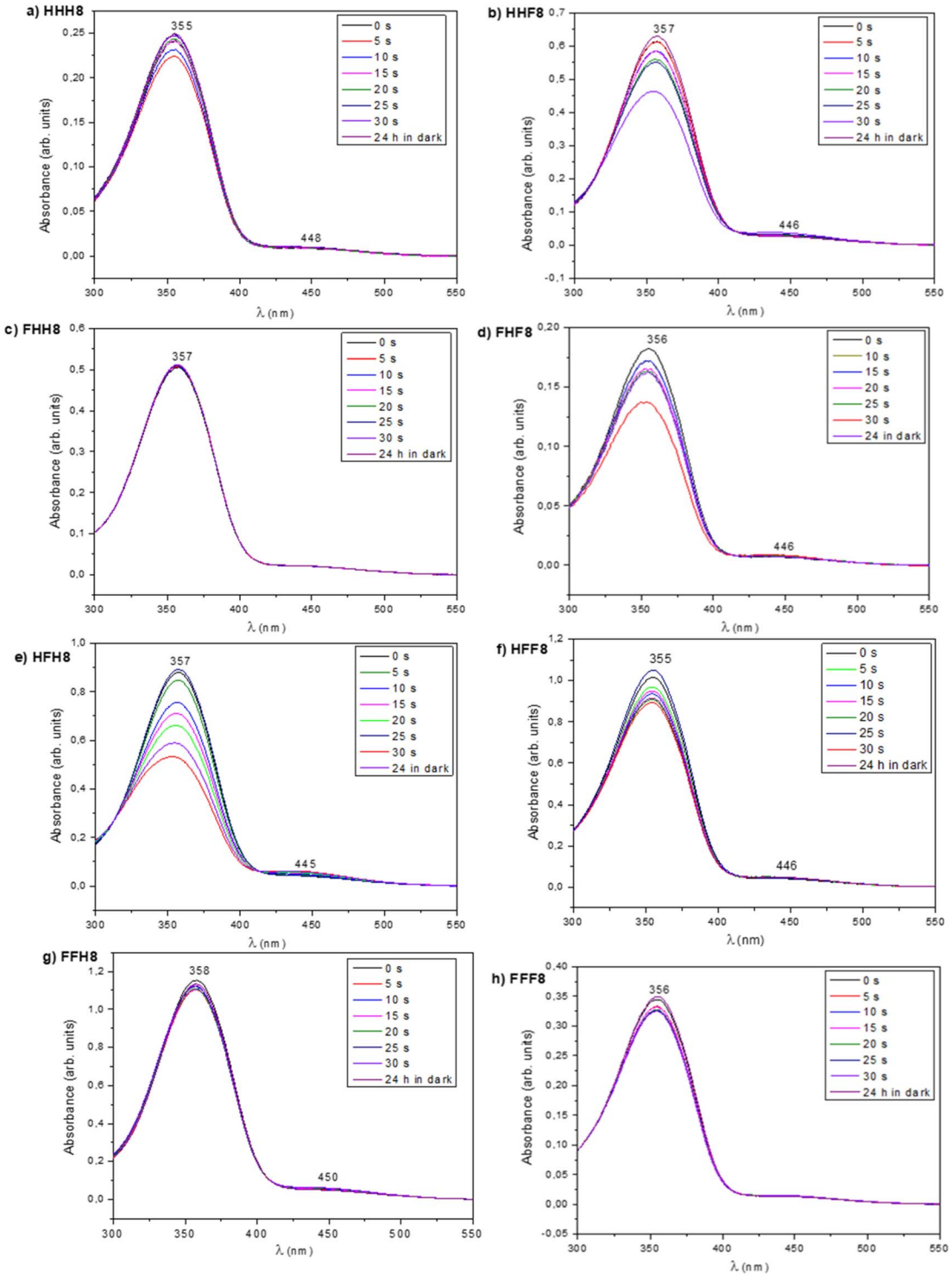

Fig. 12 Spectral changes observed under UV light irradiation for: (a) **HHH8**, (b) **HHF8**, (c) **FHH8**, (d) **FHF8**, (e) **HFH8**, (f) **HFF8**, (g) **FFH8**, (h) **FFF8** dissolved in chloroform.

substitutions in both proton donors (benzoic acid derivatives) and proton acceptors (azopyridine derivatives), we designed and synthesized eight distinct groups of HBLCs. These supramolecular complexes were thoroughly characterized using FTIR, NMR, DSC, POM, and XRD techniques, revealing a rich diversity of LC phases, including nematic, SmA, SmC, and an unidentified X phase.

An interesting finding is the identification of cybotactic nematic phases (N_{Cyb}), which are rare in rod-like LCs. The type of cybotactic clusters (N_{CybA}, N_{CybC}, or N_{CybX}) strongly depends on the adjacent LC phase, which could be modified by the

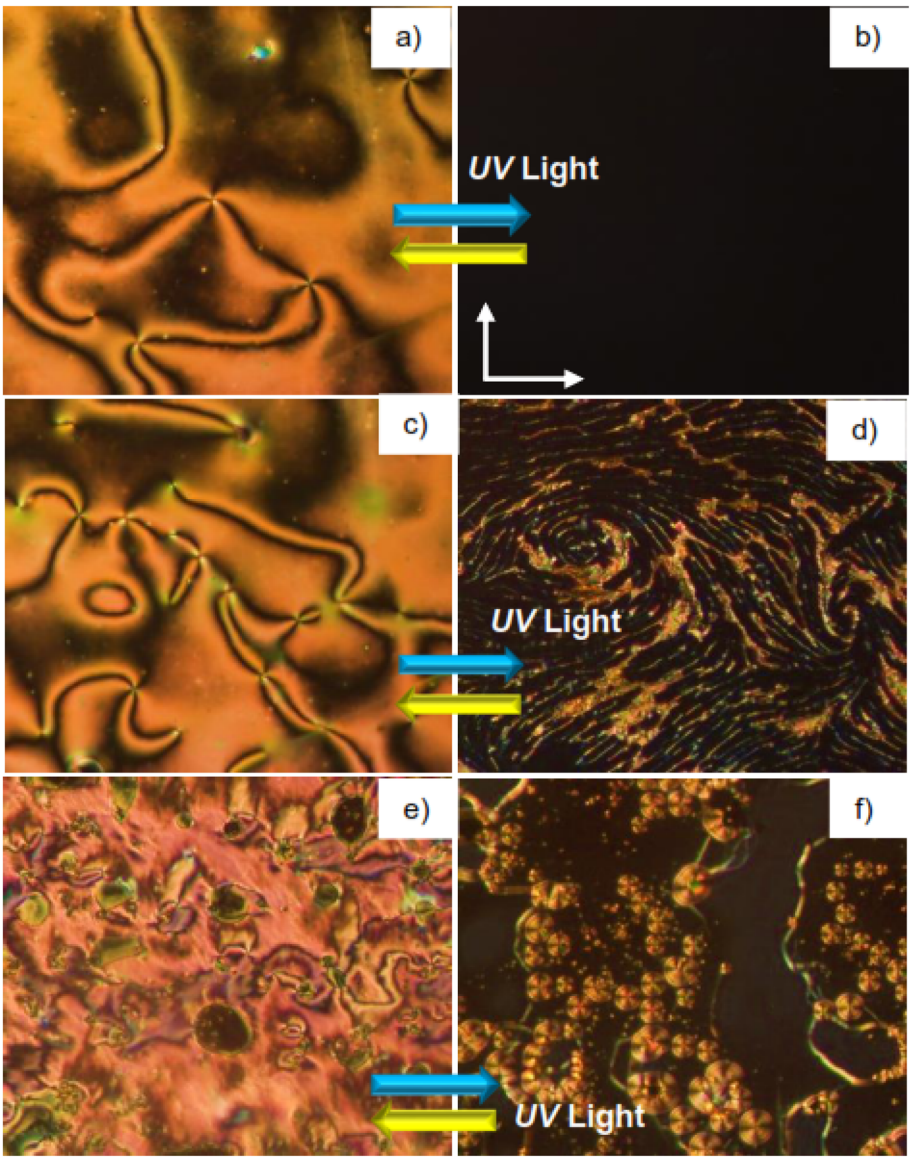

Fig. 13 Reversible isothermal photo-off–on switching between the different LC phases on cooling for: (a and b) supramolecule **HHH8** between N and isotropic phases at 125 °C, (c and d) supramolecule **FFH8** between N and SmA phases at 125 °C and (e and f) supramolecule **FFH8** between SmC and SmA at 110 °C.

degree and position of the fluorine substitution. This highlights the critical role of fluorine substitution in modulating molecular packing and intermolecular interactions. Specifically, fluorination of the benzoic acid derivatives was shown to enhance hydrogen bond strength as proved from FTIR and NMR investigations, leading to more stabilized and ordered LC phases, while fluorination of the azopyridine derivatives had a negligible effect on hydrogen bond strength but influenced phase transitions and mesophase stability.

Additionally, the photo-responsive behaviour of these HBLCs was investigated in soultion, demonstrating that the position and degree of fluorination significantly impact the rate of *trans–cis* photoisomerization. For instance, mono fluorination near the carboxylic group in the benzoic acid derivatives or at the outer side of the azopyridine derivative accelerated the photoisomerization, while double fluorination requires certain distribution of the fluorine atoms. On the other hand, the photoisomerization behaviour of triple fluorinated supramolecules was found to be comparable to the nonfluorinated ones. Regardless the degree of fluorination reversible relaxation from *cis* to *trans* isomer was found in all cases. Reversible photoswitching between LC phases (*e.g.*, SmC–SmA or N–Iso) was also achieved, showcasing the potential of these materials for applications in optical storage devices and non-linear optics.

In summary, this work not only advances our understanding of the role of aromatic core fluorination in tuning the properties of HBLCs but also provides a versatile platform for designing functional materials with tailored mesomorphic and photoresponsive behaviours avoiding many steps of organic synthesis.

Data availability

Experimental data, tables of transition temperatures and additional XRD data supporting this article have been included as part of the ESI.†

Conflicts of interest

There are no conflicts to declare.

Acknowledgements

This work was supported by the German Research Foundation (DFG) (AL2378/1-2, 424355983, RTG 2670, 436494874). A. F. Darweesh acknowledges the support by the Alexander von Humboldt Foundation for the research fellowship at Martin Luther University Halle-Wittenberg, Germany.

References

1 J. Lehn, *Supramolecular Chemistry*, Wiley, 1995.
2 J. D. Watson and F. H. C. Crick, *Nature*, 1953, **171**, 737–738.
3 J. Buchs, L. Vogel, D. Janietz, M. Prehm and C. Tschierske, *Angew. Chem.*, 2017, **129**, 286–290.
4 F. Malotke, M. Saccone, C. Wölper, R. Y. Dong, C. A. Michal and M. Giese, *Mol. Syst. Des. Eng.*, 2020, **5**, 1299–1306.
5 D. L. Nelson and M. M. Cox, *Lehninger Principles of Biochemistry*, W. H. Freeman and Company, New York, 5th edn, 2008.
6 X.-H. Cheng and H.-F. Gao, in *Hydrogen Bonded Supramolecular Materials*, Springer, Berlin, Heidelberg, 2015, pp. 133–183.
7 G. V. Oshovsky, D. N. Reinhoudt and W. Verboom, *Angew. Chem., Int. Ed.*, 2007, **46**, 2366–2370.
8 T. Kato, N. Mizoshita and K. Kanie, *Macromol. Rapid Commun.*, 2001, **22**, 797–814.
9 C. M. Paleos and D. Tsiourvas, *Liq. Cryst.*, 2001, **28**, 1127–1161.
10 T. Kato and J. M. J. Fréchet, *J. Am. Chem. Soc.*, 1989, **111**, 8533–8534.
11 B. Friot, D. Boyd, K. Willis, B. Donnio, G. Ungar and D. W. Bruce, *Liq. Cryst.*, 2000, **27**, 605–611.
12 L. Vogel, D. Janietz, M. Prehm and C. Tschierske, *Soft Matter*, 2018, **14**, 806–816.
13 N. Gimeno, M. B. Ros, J. L. Serrano and M. R. De La Fuente, *Chem. Mater.*, 2008, **20**, 1262–1271.
14 J. Wang, Y. Shi, K. Yang, J. Wei and J. Guo, *RSC Adv.*, 2015, **5**, 67357–67364.
15 M. Alaasar, C. Tschierske and M. Prehm, *Liq. Cryst.*, 2011, **38**, 925–934.
16 D. Stewart and C. T. Imrie, *Macromolecules*, 1997, **30**, 877–884.
17 M. Alaasar, X. Cai, F. Kraus, M. Giese, F. Liu and C. Tschierske, *J. Mol. Liq.*, 2022, **351**, 118597.
18 M. Alaasar, J. C. Schmidt, X. Cai, F. Liu and C. Tschierske, *J. Mol. Liq.*, 2021, **332**, 115870.
19 M. Alaasar, S. Poppe, Q. Dong, F. Liu and C. Tschierske, *Chem. Commun.*, 2016, **52**, 13869–13872.
20 M. Hird, J. W. Goodby, R. A. Lewis and K. J. Toyne, *Mol. Cryst. Liq. Cryst.*, 2003, **401**, 1–18.
21 D. Demus and H. Zaschke, *Flüssige Kristalle in Tabellen II*, veb Deutscher verlag für grundstoffindustrie, 1984.
22 T. H. Aldahri, M. Alaasar and H. A. Ahmed, *Liq. Cryst.*, 2023, **50**, 1059–1068.
23 S. Sergeyev, W. Pisula and Y. H. Geerts, *Chem. Soc. Rev.*, 2007, **36**, 1902–1929.
24 M. Powers, R. J. Twieg, J. Portman and B. Ellman, *J. Chem. Phys.*, 2022, **157**, 134901.
25 M. Alaasar, M. Prehm, M. G. Tamba, N. Sebastián, A. Eremin and C. Tschierske, *ChemPhysChem*, 2016, **17**, 278–287.
26 B. N. Sunil, M. K. Srinatha, G. Shanker, G. Hegde, M. Alaasar and C. Tschierske, *J. Mol. Liq.*, 2020, **304**, 112719.
27 H. N. S. Murthy and B. K. Sadashiva, *J. Mater. Chem.*, 2004, **14**, 2813–2821.
28 L. Caillier, E. Taffin De Givenchy, S. Géribaldi and F. Guittard, *J. Mater. Chem.*, 2008, **18**, 5382–5389.
29 S. Iamsaard, E. Anger, S. J. Aßhoff, A. Depauw, S. P. Fletcher and N. Katsonis, *Angew. Chem.*, 2016, **128**, 10062–10066.
30 J. L. Serrano, *Metallomesogens – Synthesis, Properties, and Applications*, VCH, Weinheim, Germany, 1996.
31 M. M. Zhou, J. He, H. M. Pan, Q. Zeng, H. Lin, K. Q. Zhao, P. Hu, B. Q. Wang and B. Donnio, *Chem.–Eur. J.*, 2023, **29**, e202301829.
32 F. B. Meng, X. Z. He, X. D. Zhang, Y. Ma, H. L. Han and H. Lu, *Colloid Polym. Sci.*, 2011, **289**, 955–965.
33 M. Alaasar and S. Poppe, *Liq. Cryst.*, 2020, **47**, 939–949.
34 M. A. El-Atawy, A. Z. Omar, M. L. Alazmi, M. S. Alsubaie, E. A. Hamed and H. A. Ahmed, *Heliyon*, 2023, **9**, e14871.
35 P. Kirsch, M. Bremer, M. Heckmeier and K. Tarumi, *Angew. Chem., Int. Ed.*, 1999, **38**, 1989–1992.
36 M. Poppe, C. Chen, F. Liu, S. Poppe and C. Tschierske, *Chem.–Eur. J.*, 2017, **23**, 7196–7200.
37 M. Spengler, R. Y. Dong, C. A. Michal, M. Pfletscher and M. Giese, *J. Mater. Chem. C*, 2017, **5**, 2235–2239.
38 M. Hird, *Chem. Soc. Rev.*, 2007, **36**, 2070–2095.
39 C. J. Gibb, J. Hobbs, D. I. Nikolova, T. Raistrick, S. R. Berrow, A. Mertelj, N. Osterman, N. Sebastián, H. F. Gleeson and R. J. Mandle, *Nat. Commun.*, 2024, **15**, 5845.
40 S. Brown, E. Cruickshank, J. M. D. Storey, C. T. Imrie, D. Pociecha, M. Majewska, A. Makal and E. Gorecka, *ChemPhysChem*, 2021, **22**, 2506–2510.
41 J. Karcz, J. Herman, N. Rychłowicz, P. Kula, E. Górecka, J. Szydlowska, P. W. Majewski and D. Pociecha, *Science*, 2024, **384**, 1096–1099.
42 H. Ren, P. Yang and H. Yu, *Molec*, 2022, **27**, 3977.
43 Y. Chen, H. Yu, L. Zhang, H. Yang and Y. Lu, *Chem. Commun.*, 2014, **50**, 9647–9649.
44 M. Alaasar and C. Tschierske, *Liq. Cryst.*, 2019, **46**, 124–130.
45 M. Hagar, H. A. Ahmed and O. A. Alhaddad, *Liq. Cryst.*, 2019, **46**, 1440–1451.
46 L. J. McAllister, J. Taylor, N. E. Pridmore, A. J. McEllin, A. C. Whitwood, P. B. Karadakov and D. W. Bruce, *CrystEngComm*, 2023, **25**, 1683–1692.

47 M. Alaasar, C. Anders, R. Pashameah and A. F. Darweesh, *Liq. Cryst.*, 2023, **50**, 2397–2412.
48 B. S. Ranjitha, D. Sandhya Kumari, A. Shetty, G. Shanker, M. Alaasar, R. Pashameah and G. Hegde, *J. Mol. Liq.*, 2023, **383**, 121985.
49 D. S. Kumari, A. Shetty, B. S. Ranjitha, M. Vandana, G. Shanker, M. Alaasar and G. Hegde, *Heliyon*, 2024, **10**, e37455.
50 Y. Ni, X. Li, J. Hu, S. Huang and H. Yu, *Chem. Mater.*, 2019, **31**, 3388–3394.
51 H. Yu, H. Liu and T. Kobayashi, *ACS Appl. Mater. Interfaces*, 2011, **3**, 1333–1340.
52 H. Liu, T. Kobayashi and H. Yu, *Macromol. Rapid Commun.*, 2011, **32**, 378–383.
53 M. Alaasar, J. C. Schmidt, A. F. Darweesh and C. Tschierske, *J. Mol. Liq.*, 2020, **310**, 113252.
54 M. Giese, T. Krappitz, R. Y. Dong, C. A. Michal, W. Y. Hamad, B. O. Patrick and M. J. MacLachlan, *J. Mater. Chem. C*, 2015, **3**, 1537–1545.
55 M. Spengler, R. Y. Dong, C. A. Michal, W. Y. Hamad, M. J. MacLachlan and M. Giese, *Adv. Funct. Mater.*, 2018, **28**, 1800207.
56 B. O. Lindgren and T. Nilsson, *Acta Chem. Scand.*, 1973, **27**, 888.
57 K. Schwetlick, *Organikum*, Wiley-VCH, Weinheim, Germany, 21st edn, 2001, p. 500.
58 T. Kato, J. M. J. Frechet, P. G. Wilson, T. Saito, T. Uryu, A. Fujishima, C. Jin and F. Kaneuchi, *Chem. Mater.*, 1993, **5**, 1094.
59 Y. Arakawa, Y. Sasaki and H. Tsuji, *J. Mol. Liq.*, 2019, **280**, 153–159.
60 B. S. Ranjitha, M. Alaasar and G. Shanker, *J. Mol. Struct.*, 2024, **1305**, 137626.
61 W. Nishiya, Y. Takanishi, J. Yamamoto and A. Yoshizawa, *J. Mater. Chem. C*, 2014, **2**, 3677–3685.
62 Y. Uchida, T. Akita, K. Hanada, D. Kiyohara and N. Nishiyama, *J. Mater. Chem. C*, 2022, **10**, 6621–6627.
63 Y. Kimoto, A. Nishizawa, Y. Takanishi, A. Yoshizawa and J. Yamamoto, *J. Phys. Chem. B*, 2013, **117**, 6290–6293.
64 Y. Arakawa, Y. Sasaki, K. Igawa and H. Tsuji, *New J. Chem.*, 2017, **41**, 6514–6522.
65 M. Alaasar, T. Nirgude and C. Anders, *J. Mol. Liq.*, 2024, **414**, 126174.